Chemistry & Biology
Article

Structural Proof of a Dimeric Positive Modulator Bridging Two Identical AMPA Receptor-Binding Sites

Birgitte H. Kaae,[1,3] Kasper Harpsøe,[1] Jette S. Kastrup,[1] Alberto Contreras Sanz,[2] Darryl S. Pickering,[2] Bjørn Metzler,[1] Rasmus P. Clausen,[1] Michael Gajhede,[1] Per Sauerberg,[3] Tommy Liljefors,[1] and Ulf Madsen[1,*]
[1]Department of Medicinal Chemistry
[2]Department of Pharmacology and Pharmacotherapy
Faculty of Pharmaceutical Sciences, University of Copenhagen, Universitetsparken 2, DK-2100 Copenhagen, Denmark
[3]Medicinal Chemistry Research II, Novo Nordisk A/S Novo Nordisk Park, DK-2760 Måløv, Denmark
*Correspondence: um@farma.ku.dk
DOI 10.1016/j.chembiol.2007.10.012

SUMMARY

Dimeric positive allosteric modulators of ionotropic glutamate receptors were designed, synthesized, and characterized pharmacologically in electrophysiological experiments. The designed compounds are dimers of arylpropylsulfonamides and have been constructed without a linker. The monomeric arylpropylsulfonamides were derived from known modulators and target the cyclothiazide-binding site at the AMPA receptors. The three stereoisomers—*R,R*, *meso*, and *S,S*—of the two constructed dimers were prepared, and in vitro testing showed the *R,R* forms to be the most potent stereoisomers. The biarylpropylsulfonamides have dramatically increased potencies, more than three orders of magnitude higher than the corresponding monomers. Dimer (*R,R*)-2a was cocrystallized with the GluR2-S1S2J construct, and an X-ray crystallographic analysis showed (*R,R*)-2a to bridge two identical binding pockets on two neighboring GluR2 subunits. Thus, this is biostructural evidence of a homomeric dimer bridging two identical receptor-binding sites.

INTRODUCTION

The medicinal chemistry concept of ligand dimerization is attractive for a number of reasons. The most obvious one is potentially increased affinity, because, for example, many receptors and transporters exist as dimers or higher oligomers, and dimeric ligands may bridge such oligomers. The increase in overall affinity is caused by the synergy that occurs whenever two fragments with affinity are covalently linked. The most well-known example is from the immune system, in which immunoglobulins like IgG are Nature's own dimers, linking two epitope-recognizing fragments together.

The hypothesis that the affinity of a bivalent molecule will be greater than the sum of its fragments was proposed by Page and Jencks [1, 2]. Assuming that the translational and rotational entropy of each fragment in a symmetrical dimer equals the total translational and rotational entropy for the bivalent molecule, and thus is independent of molecular weight, the loss of entropy will decrease upon joining the fragments. The sum of the affinities for two fragments binding to two identical binding sites will include two unfavorable rigid-body rotational and translational entropy contributions, whereas the affinity for a bivalent molecule in which the two fragments are linked will include only one unfavorable term. To estimate this term, Murray and Verdonk used experimental data including affinities for the fragments as well as for the molecule with the fragments joined together. The unfavorable rotational and translational entropy contribution to binding was estimated to be 15–20 kJ/mol, which corresponds to three orders of magnitude in affinity [3].

The dimerization of ligands has also served other purposes: improved pharmacokinetic properties, potency, solubility, and selectivity have been observed [4, 5]. In the early 80s, Portoghese and coworkers used the dimerization of opioid receptor ligands to demonstrate the existence of functional, dimeric G-protein-coupled receptors [6, 7]. Since then, similar approaches have been pursued in many other areas of medicinal chemistry [8].

Despite numerous examples, of which several clearly indicate that two equal binding sites are occupied by dimeric ligands, there has, so far, been no direct structural evidence for this. Here, to our knowledge, we provide the first structural evidence of a dimeric ligand that occupies two equal binding sites. The dimeric ligand was designed by using computational chemistry and targets the ionotropic glutamate receptors (iGluRs), one of the key players in neurotransmission in the brain. More specifically, the designed ligand targets the cyclothiazide (CTZ)-binding site at 2-amino-3-(3-hydroxy-5-methyl-4-isoxazolyl)propionic acid (AMPA) receptors GluR1–4. A soluble form of the extracellular ligand-binding core of GluR2 has been prepared [9], and a number of structures in complex with various agonists [9–11] and antagonists [9, 12, 13] have been determined in recent years. CTZ is a well-characterized positive allosteric modulator of AMPA receptors, and the structure of CTZ in complex with GluR2 showed that the CTZ-binding site is located at the interface between

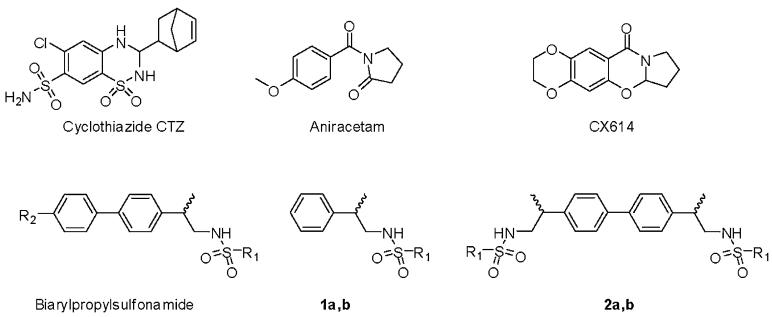

Figure 1. Known Modulators of AMPA Receptors as Well as Designed Monomeric 1a,b and Dimeric Compounds 2a,b

R_1 is either a methyl group or an isopropyl group. R_2 can be various substituents, as reported by Ornstein et al. [17].

two receptor subunits [14]. The aim of this study was to obtain potent and selective ligands, which are of great interest both as pharmacological tools and as potential therapeutics. The homodimeric ligands reported here were synthesized and pharmacologically characterized at cloned rat GluR1–4. By using X-ray crystallography, the homodimeric ligand was shown to bridge two identical CTZ-binding sites.

RESULTS AND DISCUSSION

Design

At present, crystal structures of the GluR2 ligand-binding core are available in complex with three positive allosteric AMPA receptor modulators: CTZ [14], aniracetam, and CX614 [15] (Figure 1). All three compounds bind at a two-fold symmetrical dimer interface, with the symmetry axis down through the center of the dimer interface. Two molecules of CTZ bind to two identical and symmetrical sites, which contain an N775S mutation in the GluR2 construct. These mutations cause the GluR2 construct to resemble the receptor flip splice form, which is more sensitive to CTZ. Aniracetam and CX614 bind in the region between and overlapping the two CTZ sites.

A recent computational study described a potential binding mode of a series of biarylpropylsulfonamide (Figure 1) allosteric AMPA receptor modulators [16] and utilized published structure-activity data [17]. It was hypothesized that the center of the biaryl moiety of such compounds is located close to the symmetry axis of the GluR2 dimer interface, and that the alkylsulfonamide moiety binds in one of the CTZ sites. This provided the basis for the design of a symmetrical allosteric modulator extending into both CTZ sites with a symmetrical binding mode (Figure 2).

The design of dimer **2a** (Figure 1) was based on the available structural information and the computational study mentioned above. Computational docking of **2a** was set up to test the hypothesis of a symmetrical binding mode. The crystal structure of aniracetam in complex with a GluR2 construct (PDB code: 2AL5) [15] was selected for the docking studies, because it contains specific side chain conformations expected to be important for the binding of **2a**. Previous results have shown that a biarylpropylsulfonamide modulator displays preference for the flip splice form of the AMPA receptors [18]. Assuming the same preference for compound **2a**, an amino acid replacement (N775S) was made in the structure used for docking to mimic the flip splice form. **2a** contains two chiral centers, which result in the sulfonamide hydrogen atoms and nitrogen lone pairs changing positions due to the inversion. Ensuring symmetry, the three possible configurations of **2a** were prepared and docked into the dimer interface of the GluR2 crystal structure, and the output poses showed that both the *R,R* and *S,S* stereoisomers would fit the binding site. In both cases, a symmetrical binding mode in which the biaryl moiety was located at the center of the dimer interface and the methyl sulfonamide moieties extended into the CTZ sites was observed (Figure 2). Compound **2b** (Figure 3) was designed on the basis of results obtained with monomeric modulators (Figure 1) [17]. A structurally related asymmetric analog of compound **2a** is in clinical trials [19], and, while writing this manuscript, a synthesis of this asymmetric analog was published [20].

The dockings clearly indicated that **2a** can bind in both CTZ sites in a symmetrical binding mode, and prompted

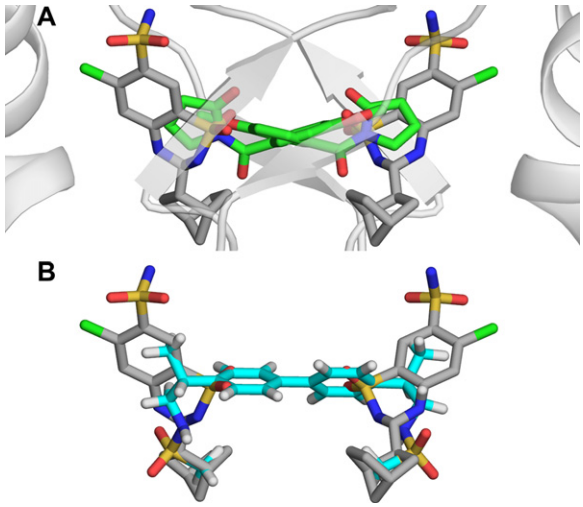

Figure 2. The Design of Dimeric Compounds

(A) Binding mode of CTZ (gray carbons) and aniracetam (green carbons: two overlapping orientations are present in the structure, each with an occupancy of 0.5) in the symmetrical dimer interface of the ligand-binding core of GluR2.

(B) Predicted binding mode of ***(R,R)*-2a** (cyan carbons) superimposed on the binding mode of CTZ (gray carbons). Compound **2b** was designed on the basis of results obtained with analogs of known biarylpropylsulfonamides (Figure 1) described by Ornstein et al. [17].

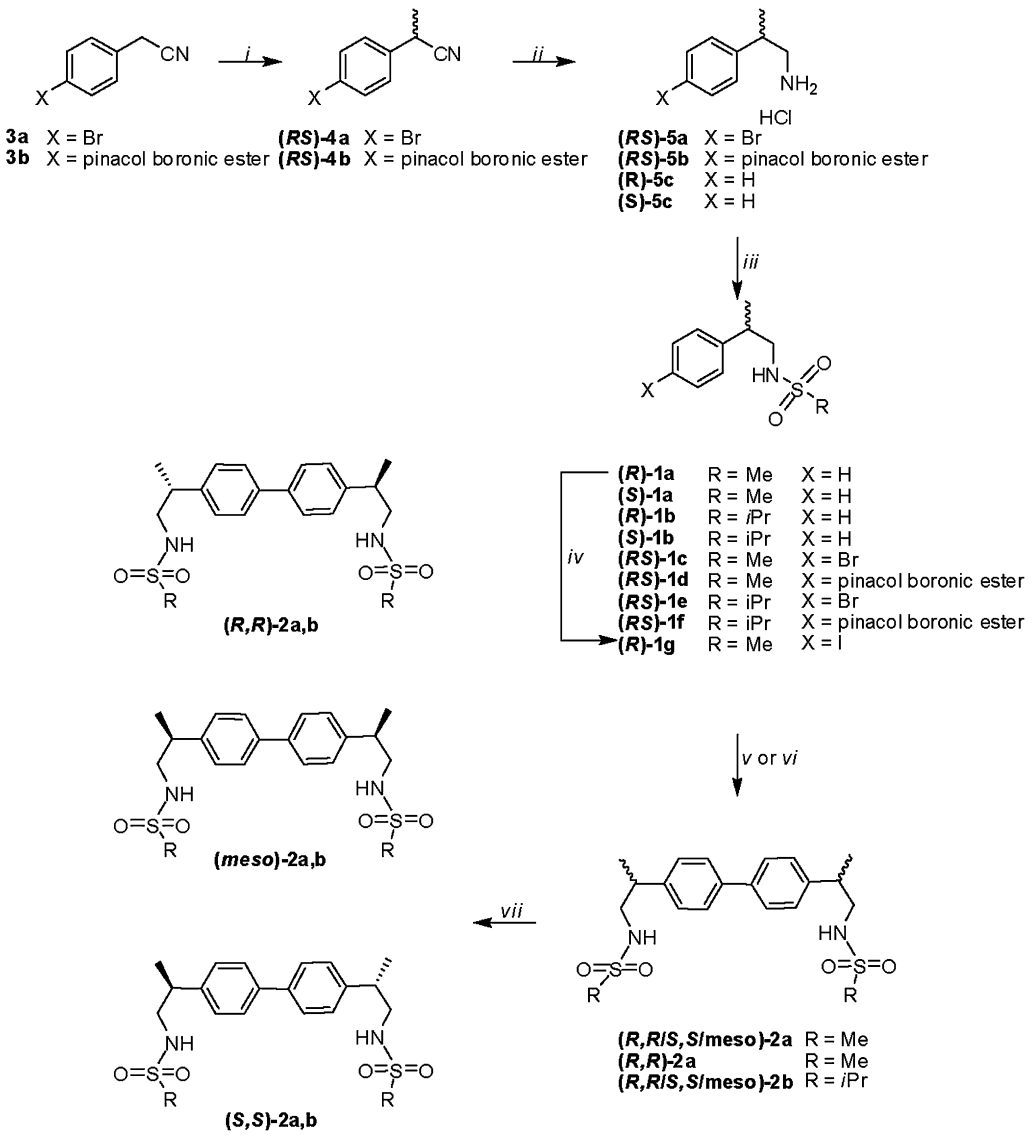

Figure 3. Synthesis of Compounds

(*i*) LiHMDS, THF, −78°C; (*ii*) BH_3•$S(CH_3)_2$, THF, reflux; (*iii*) RSO_2Cl, TEA, CH_2Cl_2, 0°C ; (*iv*) H_5IO_6, I_2, conc. H_2SO_4, AcOH, H_2O, 60°C; (*v*) Aryl halide, Aryl boronic ester, $PdCl_2(PPh_3)_2$, PPh_3, K_2CO_3, H_2O, 1.4-dioxane, 80°C; (*vi*) **1g**, LiCl, $Pd(OAc)_2$, In, DMF, 100°C; (*vii*) chiral HPLC.

us to synthesize and characterize the compounds in order to test the hypothesis.

Chemistry

The designed ligands were synthesized according to the procedures outlined in Figure 3. Optically pure **1a,b** were synthesized by using **(*R*)-** and **(*S*)-5c**, whereas **2a,b** initially were synthesized as mixtures of stereoisomers, by utilizing standard lithium-based deprotonation for the introduction of an α-methyl group on **3a,b**, followed by reduction to give **5a,b**, analogous to previously reported procedures [21]. Addition of an alkyl sulfonyl moiety afforded **1a–f**. The bivalent ligands were formed from **1c–f** via palladium-catalyzed Suzuki crosscoupling conditions and afforded **2a,b** as mixtures of stereoisomers in good yields. Using semipreparative chiral HPLC, we were able to identify systems with excellent separation (R_t = 35, 62, and 87 min for **(*R,R*)-2a**, ***meso*-2a**, and **(*S,S*)-2a**, respectively; R_t = 25, 60, and 100 min for **(*R,R*)-2b**, ***meso*-2b**, and **(*S,S*)-2b**, respectively), enabling facile separation of the stereoisomers as well as ee determinations.

Upon scaling up the syntheses, we decided to synthesize only the most potent enantiomer, **(*R,R*)-2a**, and to reduce the number of synthetic steps in order to increase the overall yield. An optically pure starting material, **(*R*)-1a**, was chosen and selectively iodinated in the *para* position, in analogy to the procedure previously reported [22] to yield **(*R*)-1g**. Direct homocoupling with indium and palladium catalysis [23] afforded **(*R,R*)-2a** in fair yield on the gram scale.

Table 1. Pharmacological Profile of the Stereoisomers of Biarylpropylsulfonamide Analogs 1a,b and 2a,b at GluR2(*Q*)$_i$ Expressed in *X. laevis* Oocytes

Compound	EC_{50} (μM)	n_H	% Max. Pot.[a]
(*R*)-1a (5)	1980 ± 285	1.37 ± 0.06	1023 ± 248
(*S*)-1a (11)	>3000	—	—
(*R*)-1b (5)	195 ± 13	1.26 ± 0.13	1097 ± 194
(*S*)-1b (6)	1485 ± 220	1.09 ± 0.04	792 ± 16
(*R,R*)-2a (9)	0.73 ± 0.13	1.36 ± 0.15	790 ± 87
***meso*-2a** (10)	0.96 ± 0.14	1.29 ± 0.09	732 ± 99
(*S,S*)-2a (8)	3.10 ± 0.46	1.36 ± 0.09	221 ± 29
(*R,R*)-2b (10)	0.44 ± 0.06	1.40 ± 0.08	796 ± 135
***meso*-2b** (8)	0.85 ± 0.18	1.61 ± 0.09	1056 ± 265
(*S,S*)-2b (11)	1.68 ± 0.27	2.66 ± 0.40	524 ± 59
CTZ (5)	5.16 ± 0.36	1.47 ± 0.04	324 ± 48

Means ± SEM are presented; the number of experiments performed (n) for each compound is indicated in parentheses. "—," immeasurable.
[a] Percentage maximum potentiation of a 10 μM (*S*)-Glu response.

Pharmacology

Profiles of Biarylpropylsulfonamide Analogs 2a,b

Recombinant rat GluR1$_i$, GluR2(Q)$_i$, GluR2(Q)$_o$, GluR3$_i$, and GluR4$_i$ were expressed in *X. laevis* oocytes; GluR2 and GluR3 contained Gly at the R/G editing site, whereas GluR1 and GluR4 contained Arg. The potentiation of (*S*)-Glu (10 μM) responses by **2a,b** was measured by using two-electrode voltage clamp electrophysiology. The activity of the enantiomers of **1a,b** was compared with that of the pure stereoisomers of **2a,b** at GluR2(*Q*)$_i$ (Table 1). CTZ was employed as a reference compound and gave an EC_{50} value (5.16 ± 0.36 μM) consistent with a previously reported value (7.6 μM) [18].

Whereas the monomeric analogs **(*R*)-1a**, **(*S*)-1a**, **(*R*)-1b**, and **(*S*)-1b** had very high or immeasurable EC_{50} values for potentiation of (*S*)-Glu responses at GluR2(*Q*)$_i$, the corresponding dimeric analogs **(*R,R*)-2a**, **(*S,S*)-2a**, ***meso*-2a**, **(*R,R*)-2b**, **(*S,S*)-2b**, and ***meso*-2b** showed very low EC_{50} values; some values were more than three orders of magnitude lower than the values for the corresponding monomer (Table 1). For **2a** and **2b**, the *R,R* enantiomers were more potent than the corresponding *S,S* enantiomers ($p < 0.05$). There was no significant difference in the potency of **(*R,R*)-2a** compared to **(*R,R*)-2b**. Potentiation by **2a** (the mixture of stereoisomers) was evaluated at holding potentials from −10 mV to −90 mV, and no voltage dependency was observed (data not shown). A comparison of the maximal potentiation produced by 30 μM **2a** (the mixture of stereoisomers) divided by the maximal potentiation given by 100 μM CTZ at GluR2(*Q*)$_i$ gave a value of 1.96 ± 0.05 (mean ± SEM, n = 14).

Subtype Selectivity of 2a

(*R,R*)-2a was evaluated for subtype selectivity (Table 2). **(*R,R*)-2a** showed only small differences in potency between the receptor subtypes GluR1$_i$–4$_i$. At GluR1$_i$ and −3$_i$, **(*R,R*)-2a** had similar potency, which was lower than that at GluR2(*Q*)$_i$ and −4$_i$. However, there was no flip versus flop selectivity when GluR2(*Q*)$_i$ and GluR2(*Q*)$_o$ were compared (Figure 4; Table 2).

X-Ray Structure Determination of *(R,R)*-2a in Complex with the Ligand-Binding Core of GluR2

As a proof of concept, we set out to crystallize **(*R,R*)-2a** in complex with the ligand-binding core of GluR2 and (*S*)-Glu by using the flip-like variant of GluR2-S1S2J (iGluR2-S1S2J-N775S) [14]. **(*R,R*)-2a** was chosen for crystallization because of a higher aqueous solubility compared to **(*R,R*)-2b**. Indeed, **(*R,R*)-2a** was found to bind at the dimer interface of GluR2-S1S2J-N775S and to bridge the two allosteric binding sites previously shown to accommodate two molecules of CTZ (Figure 5A). Thus, it was shown that the designed symmetrical allosteric modulator of GluR2 extended into both CTZ-binding sites with a symmetrical binding mode.

(*S*)-Glu introduced full domain closure (molecule A: 22.2°; molecule B: 21.0°) in GluR2-S1S2J-N775S in the presence of the allosteric modulator **(*R,R*)-2a**. The dimer-interface-accessible surface area is 760 Å^2 and is

Table 2. Pharmacological Profile of (*R,R*)-2a and (*S*)-Glu

	(*R,R*)-2a			(*S*)-Glu	
	EC_{50} (μM)	n_H	% Max. Pot.[a]	EC_{50} (μM)	n_H
GluR1$_i$	1.52 ± 0.15 (8)	2.16 ± 0.10 (8)	1,335 ± 144 (8)	12.5 ± 1.4 (9)	0.63 ± 0.07 (9)
GluR2(Q)$_i$	0.73 ± 0.13[b,c] (9)	1.36 ± 0.15 (9)	790 ± 87 (9)	14.7 ± 1.4 (13)	0.90 ± 0.04 (13)
GluR2(Q)$_o$	0.64 ± 0.13 (7)	1.30 ± 0.10 (7)	804 ± 88 (7)	1.52 ± 0.30[d] (10)	1.06 ± 0.04 (10)
GluR3$_i$	1.90 ± 0.13 (7)	2.54 ± 0.23 (7)	2,217 ± 513 (7)	21.2 ± 1.4 (11)	1.01 ± 0.02 (11)
GluR4$_i$	0.87 ± 0.11[b,c] (8)	1.80 ± 0.21 (8)	383 ± 38 (8)	19.6 ± 2.7 (14)	0.57 ± 0.01 (14)

Mean ± SEM values are presented with the n value indicated in parentheses.
[a] Percentage maximum potentiation.
[b] Statistically significantly different from GluR1$_i$ ($p < 0.05$, one-way ANOVA).
[c] Statistically significantly different from GluR3$_i$ ($p < 0.05$, one-way ANOVA).
[d] Statistically significantly different from GluR2(Q)$_i$ ($p < 0.05$, one-way ANOVA).

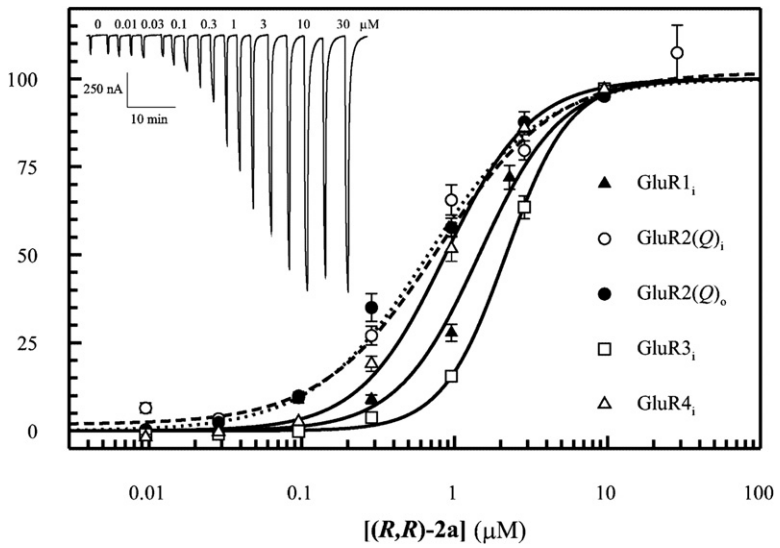

Figure 4. Pharmacology of (*R,R*)-2a
Subtype selectivity profile of **(*R,R*)-2a**. Shown are mean ± SEM responses of data pooled from all experiments by normalizing the measured potentiation to the calculated maximal potentiation for each oocyte. GluR2(Q)$_i$ (open circles, dashed line); GluR2(Q)$_o$ (closed circles, dotted line). Inset: traces from one GluR2(Q)$_i$ experiment. See Table 2 for EC_{50} values.

comprised of three regions: Ile502-Ser518, Phe679-Ile685, and Leu748-Lys782. In total, six hydrogen bonds (Leu504N[A]-Glu776OE2[B], Glu507OE1[A]-Asn768ND2 [A], and Phe512O[A]-Lys514NZ[B], and vice versa) and two salt bridges (Glu507OE1[A]-Lys514NZ[B] and vice versa) are formed between the two protomers, and this structure is similar to that of GluR2-S1S2J-N775S in complex with CTZ (PDB code: 1LBC) [14].

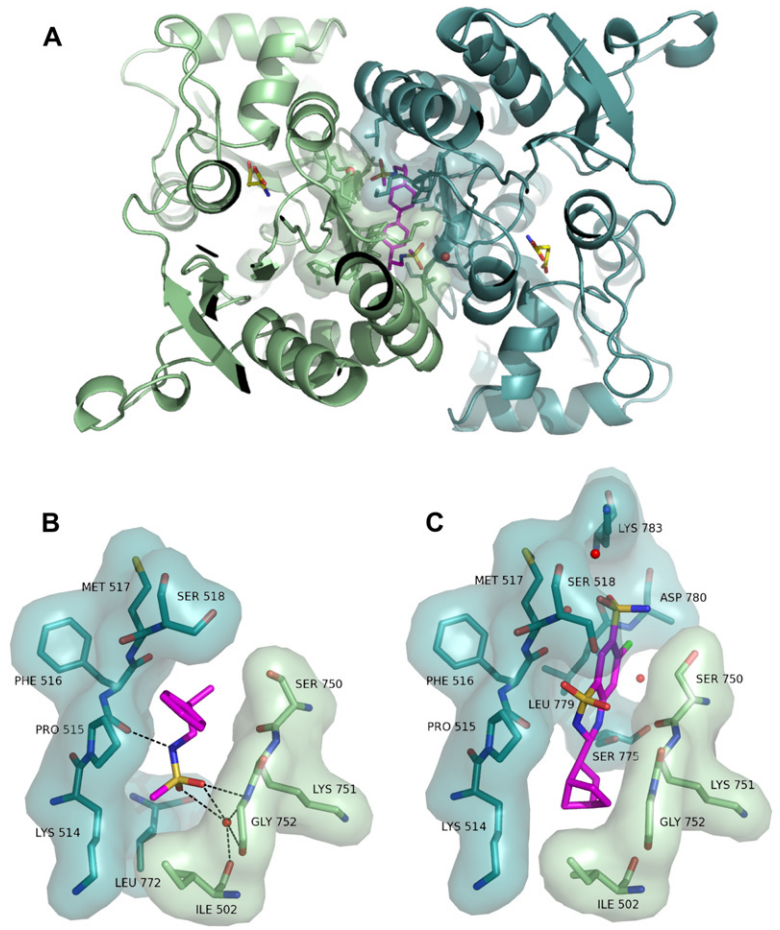

Figure 5. Bridging of Two Allosteric Binding Sites within the Ligand-Binding Core of GluR2 by (*R,R*)-2a
(A) The dimeric structure of GluR2-S1S2J-N775S in complex with (*S*)-Glu and **(*R,R*)-2a**. A ribbon representation of the two protomers comprising the dimer is shown in cyan (molecule A) and green (molecule B). Accordingly, a transparent surface representation of residues in the vicinity (max. 4 Å) of **(*R,R*)-2a** is shown. **(*R,R*)-2a** (magenta) and (*S*)-Glu (yellow) are displayed in stick representation. Two water molecules mediating interactions between **(*R,R*)-2a** and protein are shown as red spheres.
(B) Close-up view of one half of the symmetric **(*R,R*)-2a** molecule located in the binding site (shown in magenta stick representation). The view is different from that in Figure 4A). A transparent surface representation of the amino acid residues interacting with **(*R,R*)-2a** is shown (molecule A: cyan; molecule B: green). All amino acid residues within 4 Å of **(*R,R*)-2a** are shown. The atoms have been colored according to type. The interacting water molecule is shown as a red sphere. Hydrogen bonds from **(*R,R*)-2a** are displayed as stippled lines (max. 3.5 Å).
(C) Close-up view of the CTZ-binding mode in GluR2-S1S2J-N775S (PDB code: 1LBC). The view is similar to that in Figure 4B). CTZ is shown in magenta stick representation. A transparent surface representation of the residues interacting with CTZ is shown (molecule A: cyan; molecule C: green). All amino acid residues within 4 Å of CTZ are shown. The atoms have been colored according to type. The interacting water molecules are shown as red spheres.

(*R,R*)-2a binds in a symmetric manner to the two allosteric binding sites comprised of the same 10 interface residues (Ile502[B], Lys514[A], Pro515[A], Phe516[A], Met517[A], Ser518[A], Ser750[B], Lys751[B], Gly752[B], and Leu772[A], and vice versa) (Figure 5). The two sulfonamide moieties of **(*R,R*)-2a** form the same hydrogen-bonding pattern to the protein, whereas a slightly different location of the water molecule mediating hydrogen bonds between the sulfonamide oxygen atoms and the carbonyl oxygen atom of Ile502 and the nitrogen atom of Gly752 of the same protomer is seen. Hydrogen bonds are formed directly with residues Pro515 and Gly752: from the sulfonamide nitrogen atom of **(*R,R*)-2a** to the oxygen atom of Pro515 of one protomer, and from the sulfonamide oxygen atom to the nitrogen atom of Gly752 of the other protomer. Hence, the sulfonamide moiety is anchoring the allosteric modulator to both molecules comprising the dimer. The two phenyl moieties of **(*R,R*)-2a** function to bridge the two sites and make van der Waals interactions with residues Pro515-Ser518 and Ser750-Gly752 of both molecules. When comparing the structures of GluR2-S1S2J-N775S in complex with **(*R,R*)-2a** (Figure 5B) and CTZ (Figure 5C), it is evident that the sulfonamide moiety of **(*R,R*)-2a** binds at a position similar to that of the norbornene moiety of CTZ. However, the sulfonamide nitrogen atoms of the two ligands are located at equivalent positions in the two structures, which allows for hydrogen-bond formation to the same protein residue (Pro515).

SIGNIFICANCE

Positive allosteric modulators of AMPA receptors have received growing interest due to their potential clinical use for treatment of disorders such as schizophrenia, depression, and Alzheimer's disease [24]. In order to probe the hypothesis that homodimeric ligands may bind to two identical binding sites, we designed dimeric biarylpropylsulfonamides. Computational docking experiments of the methyl sulfonamide dimer 2a in the CTZ ligand-binding core of GluR2 showed a good fit in two neighboring identical binding sites, and the stereoisomers of 2a were consequently synthesized. When comparing the activity of the homodimer to the corresponding monomer, it was apparent that an increase in potency (decreased EC_{50}) of three orders of magnitude was obtained with the homodimer. As a proof-of-concept, (*R,R*)-2a was cocrystallized with the GluR2-S1S2J-N775S construct and was shown by X-ray crystallography to bridge two identical allosteric binding sites in two neighboring GluR2 subunits. Thus, this is the first, to our knowledge, structural evidence supporting the often used dimer approach within medicinal chemistry. Several explanations have been proposed for the improved pharmacological activities obtained by the dimer approach. One working hypothesis is the interaction of dimers with two neighboring identical receptor-binding sites simultaneously, and another, more likely, hypothesis is the interaction with a receptor-binding site and a secondary nonidentical binding site in the vicinity [8]. Obviously, in the present example, the mechanism for the binding of dimer (*R,R*)-2a in GluR2 is the simultaneous interaction with two identical allosteric binding sites. The design of dimeric ligands may be a generally useful way forward in the search for new, potent, selective therapeutics in the treatment of various neurological disorders.

EXPERIMENTAL PROCEDURES

Design

The GluR2-S1S2J crystal structure in complex with aniracetam [15] was retrieved from the Protein Data Bank (PDB code: 2AL5) and imported into Maestro [25]. Asn775 of both chains A and C was changed to a serine, aniracetam and water molecules were deleted, the atom types and bond orders of the agonist were corrected, and hydrogen atoms were added. The positions of polar hydrogen atoms were optimized by running the first step of refinement in the protein preparation utility of Glide [26], and a grid was prepared with the center defined by residues Pro515 and Ser518. All three midpoint box diameters were set to 14 Å, and the length of ligands was set to 10 Å. All configurations of compound **2a** were built in Maestro and were energy minimized by using MacroModel [27] with the MMFFs force field and the TNCG minimization method. The calculations were performed without a cut off distance for nonbonded interactions by using the build-in aqueous solvation model. The stereoisomers of **2a** were then docked in GluR2 by using Glide and the prepared grid, employing a scaling factor of 0.7 for all ligand atoms. The maximal output was set to 20 poses per ligand.

Synthesis and Characterization

General

All reactions involving air-sensitive reactants were performed under N_2 by using septum-syringe techniques. Glassware was flame dried under vacuum prior to use. All solvents used for air-sensitive reactions were dried over molecular sieves (3 or 4 Å) and tested on a Fisher apparatus to be below 10 ppm water. Chemicals were purchased from Fluka, Aldrich, or Frontier chemicals and were used without further purification.

^{1}H-NMR and ^{13}C-NMR spectra were recorded on a Varian Mercury (300 MHz), a Varian Gemini (300 MHz), or a DRX (300 or 400 MHz) spectrometer in $CDCl_3$, CD_3OD, or DMSO-d6 by using either TMS or solvent as the internal standard. Chemical shifts (δ) are expressed in ppm and coupling constants (*J*) in Hertz. Optical rotation was measured on a Perkin Elmer 241 Polarimeter. Commercially available TLC plates (silica gel 60 F_{254}) were used for TLC analyses, and the spots were visualized by using UV light (254 nm) or either an alkaline potassium permanganate or a ninhydrin solution for soaking the plates. Melting points were determined in open capillaries by using a Buchi B-545 melting point apparatus or a SRS Optimelt MPA100 apparatus and are uncorrected. Microanalyses were performed by Mikro Kemi AB, Seminariegatan, Uppsala, Sweden or by J. Theiner, Microanalytical Laboratory, Dept. of Physical Chemistry, University of Vienna, Austria and agree with the theoretical values ±0.4%.

(R,S)-2-(4-Bromophenyl)Propanenitrile, (R,S)-4a

4-Bromobenzylacetonitrile (**3a**) (9.00 g; 45.91 mmol) was dissolved in THF (60 ml; 0.75 M solution) and cooled to −78°C, and LiHMDS (48.20 ml 1 M in THF; 48.20 mmol) was added dropwise while stirring. Stirring was continued at −78°C for 1 hr before the addition of iodomethane (3.01 ml; 6.84 g; 48.20 mmol). The reaction was stirred at −78°C for another hour before it was allowed to warm to room temperature overnight. The reaction was poured into H_2O (900 ml), acidified with 1 M HCl, and extracted with EtOAc (3 × 600 ml). The combined organic phases were washed with H_2O (150 ml) and brine (150 ml), dried ($MgSO_4$), and filtered, and the solvent was evaporated to yield

(RS)-4a as a red oil (9.26 g; 96%). ^{1}H-NMR (300 MHz) in $CDCl_3$ δ 1.65 (d, *J* = 6 Hz, 3H); 3.87 (q, *J* = 6 Hz, 1H); 7.22 (d, *J* = 9 Hz, 2H); 7.50 (d, *J* = 9 Hz, 2H); ^{13}C-NMR (100 MHz) in $CDCl_3$ δ 21.69; 29.40; 127.31; 128.86; 130.25; 132.33; 132.67.

(R,S)-2-(4-[4,4,5,5-Tetramethyl-1,3,2-Dioxaborolan-2-yl]Phenyl)Propanenitrile, *(R,S)-4b*

(R,S)-4b was synthesized and purified analogously to **(R,S)-4a** by using 2-(4-[4,4,5,5-tetramethyl-1-3-2-dioxaborolan-2-yl]phenyl) acetonitrile (10.00 g; 41.13 mmol) as starting material. Crude **(R,S)-4b** was obtained as a yellow oil that crystallized upon standing, mp 80.5°C–81.0°C (10.51 g; 99%). ^{1}H-NMR (300 MHz) in $CDCl_3$ δ 1.35 (s, 12H); 1.64 (d, *J* = 6 Hz, 3H); 3.90 (q, *J* = 6 Hz, 1H); 7.37 (d, *J* = 9 Hz, 2H); 7.83 (d, *J* = 9 Hz, 2H); ^{13}C-NMR (75 MHz) in $CDCl_3$ δ 21.45; 24.86; 31.42; 83.99; 121.38; 126.04; 134.92; 135.60; 139.97.

(R,S)-2-(4-Bromophenyl)Propan-1-Amine Hydrochloride, *(R,S)-5a*

(R,S)-4a (3.95 g; 18.80 mmol) was dissolved in THF (0.5 M solution), and BH_3•$S(CH_3)_2$ (10.34 ml; 2 M in THF, 20.68 mmol) was added. The reaction was heated to reflux for 3 hr. After cooling to room temperature, the reaction was treated with sat. HCl in Et_2O until precipitation started. Filtration and drying afforded pure **(R,S)-5a** as white crystals, mp 201.5°C–202.9°C, (4.69 g; 99%). ^{1}H-NMR (300 MHz) in DMSO-d_6 δ 1.26 (d, *J* = 6 Hz, 3H); 2.93–3.12 (m, 1H); 3.48–3.54 (m, 1H); 3.66–3.74 (m, 1H); 7.28 (d, *J* = 6 Hz, 2H); 7.50 (d, *J* = 6 Hz, 2H); 8.08 (bs, 2H); ^{13}C-NMR (75 MHz) in DMSO-d_6 δ 19.51; 37.24; 44.95; 120.31; 129.96; 131.83; 142.56.

(R,S)-2-(4-[4,4,5,5-Tetramethyl-1,3,2-Dioxaborolan-2-yl]Phenyl)Propan-1-Amine Hydrochloride, *(R,S)-5b*

(R,S)-5b was synthesized analogously to **5a** by using **4b** (4.35 g; 16.92 mmol) as starting material. Pure **(R,S)-5b** was obtained as white crystals, mp 79.5°C–80.5°C (5.01 g; 99%). ^{1}H-NMR (300 MHz) in $CDCl_3$ δ 1.25–1.32 (m, 15 H); 2.94–3.12 (m, 1H); 3.45–3.51 (m, 1H); 3.66–3.73 (m, 1H); 7.34 (d, *J* = 6 Hz, 2H); 7.65 (d, *J* = 6 Hz, 2H); 8.04 (bs, 2H); ^{13}C-NMR (100 MHz) in $CDCl_3$ δ 22.44; 27.74; 40.75; 46.88; 86.86; 129.49; 130.08; 138.12; 147.98.

General Method for Addition of Alkane Sulfonyl Chloride to Primary Amines to Give *(R,S)-1a–f*

2-Phenyl-1-propylamine or 2-phenyl-1-propylamine hydrochloride (1 eq.) was dissolved or suspended in CH_2Cl_2 (0.25 M solution) and cooled to 0°C, and TEA (20% v/v with respect to CH_2Cl_2) was added. Methyl or isopropyl sulfonyl chloride (1.5 eq.) was added dropwise, and the reaction was stirred at 0°C for 1 hr at room temperature overnight. The reaction was diluted with Et_2O to 5× the volume, and the reaction was washed once with H_2O, 0.2 M HCl, sat. $NaHCO_3$, and brine. The organic phase was dried (Na_2SO_4), filtered, and evaporated to yield crude **(R,S)-1a–f** as oils.

(R)-N-(2-Phenylpropyl)Methanesulfonamide, *(R)-1a*

(R)-1a was synthesized according to the general method with **(R)-5c** (6.00 g; 44.38 mmol) and methyl sulfonyl chloride (5.17 ml; 7.63 g; 66.57 mmol). Crude **(R)-1a** was purified via reverse-phase preparative HPLC (Xterra column, water [0.1% TFA] and a CH_3CN gradient of 5%–95% over the course of 20 min). **(R)-1a** was obtained as a clear, slightly yellow oil (9.21 g; 97%). $[\alpha]^{24}_{589}$ = +5.6° (*c* 0.16, CH_2Cl_2). ^{1}H-NMR (300 MHz) in $CDCl_3$ δ 1.36 (d, *J* = 9 Hz, 3H); 2.77 (s, 3H); 2.98–3.05 (m, 1H); 3.25–3.38 (m, 2H); 4.74 (bs, 1H); 7.26–7.41 (m, 5H); ^{13}C-NMR (75 MHz) in $CDCl_3$ δ 19.58; 40.50; 50.46; 53.46; 127.35; 127.71; 129.17; 143.70. Analysis CHN($C_{10}H_{15}NO_2S$•0.5 H_2O, 0.15 $C_2HO_2F_3$).

(S)-N-(2-Phenylpropyl)Methanesulfonamide, *(S)-1a*

(S)-1a was synthesized according to the general method with **(R)-5c** (1.00 g; 7.40 mmol) and methyl sulfonyl chloride (0.86 ml; 1.27 g; 11.09 mmol). Crude **(S)-1a** was purified via FC (silica 60; eluent: heptane with rising EtOAc gradient) to afford **(S)-1a** as clear, slightly yellow oil (1.18 g; 75%). $[\alpha]^{23}_{589}$ = −9.0° (*c* 0.75, CH_2Cl_2). ^{1}H-NMR (300 MHz) in $CDCl_3$ δ 1.32 (d, *J* = 9 Hz, 3H); 2.78 (s, 3H); 2.90–3.02 (m, 1H); 3.20–3.28 (m, 1H); 3.35–3.42 (m, 1H); 4.15 (bs, 1H); 7.20–7.36 (m, 5H); ^{13}C-NMR (100 MHz) in $CDCl_3$ δ 19.00; 40.31; 49.96; 53.46; 127.13; 127.28; 128.91; 142.02. Analysis CHN($C_{10}H_{15}NO_2S$).

(R)-N-(2-Phenylpropyl)Propane-2-Sulfonamide, *(R)-1b*

(R)-1b was synthesized according to the general method with **(R)-5c** (1.00 g; 7.40 mmol) and isopropyl sulfonyl chloride (1.26 ml; 1.61 g; 12.13 mmol). Crude **(R)-1b** was purified via reverse-phase preparative HPLC (Xterra column, water [0.1% TFA] and a CH_3CN gradient of 5%–95% over the course of 20 min). **(R)-1b** was obtained as a clear, slightly yellow oil (1.71 g; 96%). $[\alpha]^{24}_{589}$ = +7.3° (*c* 0.17, CH_2Cl_2). ^{1}H-NMR (400 MHz) in $CDCl_3$ δ 1.29 (d, *J* = 12 Hz, 3H); 1.32 (d, *J* = 9 Hz, 6H); 2.93–3.07 (m, 2H); 3.18–3.27 (m, 1H); 3.34–3.42 (m, 1H); 4.01 (bs, 1H); 7.20–7.27 (m, 3H); 7.33 (t, *J* = 6 Hz, 2H); ^{13}C-NMR (100 MHz) in $CDCl_3$ δ 14.71; 14.87; 16.98; 39.13; 48.32; 51.61; 125.24; 125.37; 127.09; 142.00. Analysis CHN($C_{12}H_{19}NO_2S$•0.25 H_2O).

(S)-N-(2-Phenylpropyl)Propane-2-Sulfonamide, *(S)-1b*

(S)-1b was synthesized according to the general method with **(R)-5c** (1.00 g; 7.40 mmol) and isopropyl sulfonyl chloride (1.24 ml; 1.58 g; 11.94 mmol). Crude **(S)-1b** was purified by using FC (silica 60; eluent: heptane with rising EtOAc gradient) and afforded **(S)-1b** as a clear oil (1.43 g; 80%). $[\alpha]^{25}_{589}$ = −11.1° (*c* 0.55, CH_2Cl_2). ^{1}H-NMR (400 MHz) in $CDCl_3$ δ 1.25 (d, *J* = 12 Hz, 3H); 1.30 (d, *J* = 9 Hz, 6H); 2.98–3.08 (m, 2H); 3.16–3.26 (m, 1H); 3.32–3.41 (m, 1H); 4.02 (bs, 1H); 7.21—7.28 (m, 3H); 7.34 (t, *J* = 6 Hz, 2H); ^{13}C-NMR (100 MHz) in $CDCl_3$ δ 14.53; 14.66; 17.16; 38.84; 48.39; 51.37; 125.17; 125.32; 126.99; 141.12. Analysis CHN($C_{12}H_{19}NO_2S$•0.10 H_2O•0.10 $C_2HF_3O_2$).

(R,S)-N-(2-[4-Bromophenyl]Propyl)Methanesulfonamide, *(R,S)-1c*

(R,S)-1c was synthesized according to the general method with **(R,S)-5a** (2.35 g; 9.38 mmol) and methyl sulfonyl chloride (1.28 ml; 1.89 mg; 16.46 mmol). **(R,S)-1c** was obtained as a red-brown oil (2.71 g, 99%), which could be used without further purification. ^{1}H-NMR (400 MHz) in $CDCl_3$ δ 1.28 (d, *J* = 9 Hz, 3H); 2.82 (s, 3H); 2.92–3.03 (m, 3H); 4.09 (bs, 1H); 7.10 (d, *J* = 9 Hz, 2H); 7.46 (d, *J* = 9 Hz, 2H); ^{13}C-NMR (100 MHz) in $CDCl_3$ δ 18.86; 39.99; 40.49; 49.74; 121.00; 129.03; 132.03; 141.94. Analytical purification: CF (silica 60 H, eluent: heptane with rising EtOAc gradient) yielded pure **(R,S)-1c**, which crystallized upon standing, mp = 74.5°C–75.5°C. Analysis CHN($C_{10}H_{14}BrNO_2S$).

(R,S)-N-(2-[4-(4,4,5,5-Tetramethyl-1,3,2-Dioxaborolan-2-yl)Phenyl]Propyl)Methanesulfonamide, *(R,S)-1d*

(R,S)-1d was synthesized according to the general method with **(R,S)-5b** (4.42 g; 14.85 mmol) and methyl sulfonyl chloride (1.97 ml; 2.91 g; 25.36 mmol). Crude **(R,S)-1d** was obtained as a yellow oil (4.89 g; 97%) and was used without further purification. ^{1}H-NMR (400 MHz) in $CDCl_3$ δ 1.30 (d, *J* = 12 Hz, 3H); 1.35 (s, 12H); 2.79 (s, 3H); 2.83–3.08 (m, 1H); 3.21–3.29 (m, 1H); 3.33–3.43 (m, 1H); 7.24 (d, *J* = 6 Hz, 2H); 7.77 (d, *J* = 6 Hz, 2H); ^{13}C-NMR (100 MHz) in $CDCl_3$ δ 18.91; 21.07; 31.53; 40.38; 49.79; 83.85; 126.69; 135.46; 146.17.

(R,S)-N-(2-[4-Bromophenyl]Propyl)Propane-2-Sulfonamide, *(R,S)-1e*

(R,S)-1e was synthesized according to the general method with **(R,S)-5a** (3.60 g; 14.37 mmol) and isopropyl sulfonyl chloride (2.82 ml; 3.60 g; 25.22 mmol). **(R,S)-1e** was obtained as a yellow, semicrystalline substance (4.37 g; 95%). ^{1}H-NMR (400 MHz) in $CDCl_3$ δ 1.18–1.34 (m, 9H); 2.70–3.48 (m, 4H); 7.09 (dd, *J* = 6 and 3 Hz, 2H); 7.47 (dd, *J* = 6 and 3 Hz, 2H); ^{13}C-NMR (100 MHz) in $CDCl_3$ δ 16.63; 18.92; 40.49; 50.20; 53.57; 120.86; 129.12; 131.99; 142.08.

(R,S)-N-(2-[4-(4,4,5,5-Tetramethyl-1,3,2-Dioxaborolan-2-yl)Phenyl]Propyl)Propane-2-Sulfonamide, *(R,S)-1f*

(R,S)-1f was synthesized according to the general method with **(R,S)-5b** (4.00 g; 13.44 mmol) and isopropyl sulfonyl chloride (2.57 ml; 3.28 g; 22.97 mmol). Crude **(R,S)-1f** was obtained as a yellow, semicrystaline substance (4.00 g; 81%). ^{1}H-NMR (400 MHz) in $CDCl_3$ δ 1.32 (m, 12H); 1.31–1.37 (m, 2H); 2.74–3.39 (m, 4H); 7.23 (dd, *J* = 6 and 3 Hz, 2H); 7.78 (dd, *J* = 6 and 3 Hz, 2H); ^{13}C-NMR (100 MHz) in $CDCl_3$ δ 14.21; 21.07; 24.86; 43.70; 60.41; 69.22; 83.71; 126.85; 135.10; 146.88.

(R)-N-(2-[4-Iodophenyl]Propyl)Methanesulfonamide, *(R)-1g*

(R)-1a (8.0 g; 37.5 mmol) was dissolved in AcOH (44 ml) and was treated with conc. H_2SO_4 (4.0 g; 2.22 ml) and H_2O (9.0 ml) while stirring.

To this solution, H_5IO_6 (2.14 g; 9.38 mmol) was added, followed by I_2 (4.76 g; 18.75 mmol), and the reaction was heated to 60°C for 3 hr. The reaction was allowed to reach 30°C and esd added dropwise to a solution of $NaHSO_3$ (2.0 g) in sat. $NaHCO_3$ (30 ml). The aqueous solution was extracted with EtOAc (3 × 100 ml), and the combined organic phases were dried ($MgSO_4$). Hot (80°C) heptane (300 ml) was added, and the EtOAc:heptane phase was concentrated under reduced pressure at 70°C to a total volume of 300 ml, at which point crystals appeared. The reaction was left for 18 hr to allow precipitation of **(*R*)-1g**. The crystals were filtered off, washed with heptane, and dried to afford crude **(*R*)-1g**. According to ^{1}H-NMR, ~10% unconverted **(*R*)-1a** was observed in the sample. Crude **(*R*)-1g** (12.01 g, 85%, corrected according to NMR) was used without further purification. Mp 99°C–100C. ^{1}H-NMR (300 MHz) in $CDCl_3$ 1.45 (d, J = 6 Hz, 3H); 3.00 (s, 3H); 3.34–3.52 (m, 3H); 4.38 (bs, 1H); 7.15 (d, J = 9 Hz, 2H); 7.84 (d, J = 9 Hz, 2H); ^{13}C-NMR (75 MHz) in $CDCl_3$ δ 19.37; 40.58; 40.97; 50.18; 92.73; 129.68; 138.29; 142.97.

(R,R)-, (S,S)-, and (Meso)-N,N-(2,2′-[Biphenyl-4-4′-Diyl]Bis[Propane-2,1-Diyl])Dimethanesulfonamide, *2a*

(*R,S*)-1c (2.43 g; 8.32 mmol) was dissolved in 1.4-dioxane (0.05 M), and $PdCl_2(PPh_3)_2$ (292 mg; 0.42 mmol; 5 mol%) and PPh_3 (100 mg; 0.38 mmol; 5 mol%) were added. The mixture was stirred for 15 min before the addition of K_2CO_3 (5.75 g; 41.58 mmol), **(*R,S*)-1d** (3.53 g; 10.40 mmol), and H_2O (equal amount to 1.4-dioxane). The reaction was heated to 80°C for 4 days and allowed to cool to room temperature. H_2O (475 ml) was added, and the mixture was extracted with Et_2O (3 × 450 ml). The combined organic phases were washed with H_2O (150 ml), 1 M NaOH (150 ml), and H_2O (150 ml). Drying (Na_2SO_4), filtration, and evaporation of the solvent afforded crude **2a** as a light-yellow oil. CF (silica 60 H, eluent: heptane with rising EtOAc gradient) yielded **2a** as a white, crystalline powder containing a mixture of stereoisomers (937 mg; 86%). Mp 165°C–174°C. ^{1}H-NMR (400 MHz) in $CDCl_3$ δ 1.36 (d, J = 9 Hz, 6H); 2.84 (s, 6H); 3.00–3.11 (m, 2H); 3.24–3.35 (m, 2H); 3.38–3.47 (m, 2H); 4.14 (bs, 2H); 7.31 (d, J = 6 Hz, 4H); 7.57 (d, J = 6 Hz, 4H); ^{13}C-NMR (100 MHz) in $CDCl_3$ δ 19.02; 40.05; 40.40; 49.91; 127.55; 127.78; 139.60; 142.02. **2a** mixture of stereoisomers: analysis CHN($C_{20}H_{28}N_2O_4S_2$•0.30 C_7H_{16}•0.25 $C_2HF_3O_2$).

Chiral HPLC purification with a Daicel Chiralpak AS (2 × 25 cm) column and 50:50 heptane:ethanol with a 7.00 ml/min flow afforded the pure stereoisomers: R_t**(*R,R*)-2a** = 35 min, R_t**(*meso*)-2a** = 60 min, and R_t**(*S,S*)-2a** = 87 min (for details, see the Supplemental Data available with this article online). **(*R,R*)-2a**: $[\alpha]^{25}_{589}$ = +48° (*c* 0.115, CH_2Cl_2); ***meso*-2a**: $[\alpha]^{25}_{589}$ = +2.1° (*c* 0.095, CH_2Cl_2); **(*S,S*)-2a**$[\alpha]^{25}_{589}$ = −50° (*c* 0.170, CH_2Cl_2). **(*R,R*)-2a**: mp 207.6°C–208.0°C; **(*meso*)-2a**: mp 192.7°C–193.1°C; **(*S,S*)-2a**: mp 202.3°C–203.8°C. Analysis **(*R,R*)-2a**: CHN($C_{20}H_{28}N_2O_4S_2$•0.10 C_7H_{16}•0.10 $C_2HF_3O_2$); **(*meso*)-2a**: CHN($C_{20}H_{28}N_2O_4S_2$•0.15 C_7H_{16}•0.15 $C_2HF_3O_2$); **(*S,S*)-2a**: CHN($C_{20}H_{28}N_2O_4S_2$•0.20 C_7H_{16}•0.25 $C_2HF_3O_2$).

(R,R)-, (S,S)-, and (Meso)-N,N-(2,2′-[Biphenyl-4-4′-Diyl]Bis[Propane-2,1-Diyl])Dipropane-2-Sulfonamide, *2b*

2b was synthesized and purified analogously to **2a** by using **(*RS*)-1e** (1.70 g; 5.31 mmol) and **(*RS*)-1f** (2.44 g; 6.64 mmol). **2b** was obtained as an off-white, crystalline powder containing all three stereoisomers (2.98 g, 56%), mp > 210°C. ^{1}H-NMR (300 MHz) in $CDCl_3$ δ 1.12–1.33 (m, 18H); 2.97–3.12 (m, 4H); 3.21–3.30 (m, 2H); 3.37–3.44 (m, 2H); 3.90 (bs, 2H); 7.29 (d, J = 9 Hz, 4H); 7.56 (d, J = 9 Hz, 4H); ^{13}C-NMR (100 MHz) in $CDCl_3$ δ 16.64; 19.10; 40.52; 50.33; 53.53; 127.52; 127.82; 139.58; 142.14. Chiral HPLC purification with a Daicel Chiralpak AD (2 × 25 cm) column and 40:60 heptane:EtOH with a 7.00 ml/min flow afforded the pure stereoisomers: R_t**(*R,R*)-2b** = 25 min, R_t**(*meso*)-2b** = 62 min, and R_t**(*S,S*)-2b** = 100 min (for details, see the Supplemental Data). **(*R,R*)-2b**: $[\alpha]^{25}_{589}$ = +31° (*c* 0.089, CH_2Cl_2); ***meso*-2b**: $[\alpha]^{25}_{589}$ = −0.7° (*c* 1.156, CH_2Cl_2); **(*S,S*)-2b**: $[\alpha]^{25}_{589}$ = −33° (*c* 0.103, CH_2Cl_2). **(*R,R*)-2b** and ***meso*-2b** were further recrystallized from EtOAc:toluene. Analysis **(*R,R*)-2b**: CHN($C_{24}H_{36}N_2O_4S_2$•0.65 C_7H_8•0.10 $C_2HF_3O_2$); **(*meso*)-2b**: CHN ($C_{24}H_{36}N_2O_4S_2$•0.36 C_7H_8•0.24 $C_2HF_3O_2$); **(*S,S*)-2b**: CHN($C_{24}H_{36}N_2O_4S_2$•0.60 C_7H_{16}•0.15 $C_2HF_3O_2$).

(R,R)-N,N-(2,2′-[Biphenyl-4-4′-Diyl]Bis[Propane-2,1-Diyl])Dimethanesulfonamide, *(R,R)-2a*

(*R*)-1g (4.0 g 90% pure; 10.6 mmol, corrected), LiCl (665 mg; 15.6 mmol), $Pd(OAc)_2$ (59 mg; 0.27 mmol), In (600 mg; 5.30 mmol), and DMF (20 ml) were mixed and stirred 1 hr at 100°C. TLC (eluted with EtOAc) revealed ~50% unconverted **(*R*)-1g**. Additional $Pd(OAc)_2$ (30 mg; 0.13 mmol) and In (300 mg; 2.65 mmol) were added, and stirring was continued at 100°C for 1 hr, after which no **(*R*)-1g** could be seen, as judged by TLC. The reaction was allowed to cool to room temperature, and H_2O (50 ml) was added. The aqueous solution was extracted with EtOAc (3 × 100 ml), and the combined organic phases were dried ($MgSO_4$) and filtered through silica (35–70 μm, 1 cm layer). The filtrate was heated to 70°C, and hot heptane (80°C, 300 ml) was added. Precipitation was initiated by concentration in vacuo at 70°C of the volume to a total of 300 ml, and the reaction was left to crystallize for 24 hr before filtration to yield **(*R,R*)-2a** (0.970 g, 43%), mp 202.6°C–203.4°C. $[\alpha]^{25}_{589}$ = +50° (*c* 0.156, CH_2Cl_2); ^{1}H-NMR (300 MHz) and ^{13}C-NMR (75 MHz) in $CDCl_3$ are identical to data obtained for **2a**. Analysis CHN($C_{10}H_{15}NO_2S$•0.35 $C_4H_8O_2$).

Pharmacology

Molecular Biology

The rat AMPA receptor clones GluR1–4 in the vector pGEMHE [28] were used for preparation of high-expression cRNA transcripts for functional expression in oocytes. cDNAs were grown in XL1 Blue bacteria (Stratagene, La Jolla, CA) and were prepared by using column purification (QIAGEN, Chatsworth, CA). cRNA was synthesized from cDNA by using the mMessage mMachine T7 transcription kit (Ambion, Inc., Austin, TX) and were purified by using RNeasy spin columns (QIAGEN). Restriction and other molecular biological enzymes were obtained from New England BioLabs (Beverly, MA).

Two-Electrode Voltage Clamp Electrophysiology

X. laevis oocytes were obtained as previously detailed [29]. Recordings were made at room temperature at holding potentials in the range of −10 to −90 mV, whereas the oocytes were continuously superfused with Ca^{2+}-free frog Ringer's solution (in mM: 115 NaCl, 2 KCl, 1.8 $BaCl_2$, 5 HEPES [pH 7.0]). Potentiating compounds were dissolved in DMSO or DMSO:ethanol (1:1) as 10–30 mM stock solutions, which were stored at −30°C and were freshly diluted into Ca^{2+}-free frog Ringer's solution. (*S*)-Glu (10 μM) was freshly prepared from frozen 500 mM stock solutions. Drugs were coapplied with (*S*)-Glu and were added by bath application for 30–60 s until a plateau response was obtained. The percent potentiation at each concentration of potentiator was calculated as the percentage increase in the control current (that given by 10 μM (*S*)-Glu, which is near the EC_{50} value at all of the flip receptors studied).

Data Analysis

Concentration-response curves for potentiators were analyzed by using Grafit v3.00 (Erithacus Software Ltd., Horley, UK) to determine the EC_{50}, Hill value (n_H), and percent maximum potentiation (%P_{max}) with a logistic equation: $\%P = \%P_{max}/(1 + [10^{(\log[EC50])}/10^{(\log[Drug])}]^{nH})$, where %P is the measured percent potentiation. SigmaStat v3.11 (SSI, San Jose, CA) was employed for the statistical analysis of pharmacological data. One-way ANOVA with a Bonferroni posttest was used for statistical comparison of measured parameters, which were considered significantly different if $p < 0.05$. For graphical representation of concentration-response data, responses were pooled from all experiments at a given receptor and potentiator by normalizing the percent potentiation at each drug concentration to the calculated maximal potentiation at each individual oocyte.

X-Ray Structure Determination

The point mutation N775S was introduced into the GluR2-S1S2J construct developed by Armstrong and Gouaux [9], thereby converting the GluR2-S1S2J flop splice form into a flip-like variant. The GluR2-S1S2J-N775S protein was expressed, refolded, and purified essentially as previously reported [30, 31], with 1 mM (*S*)-Glu present during all steps.

GluR2-S1S2J-N775S was crystallized in complex with (*S*)-Glu and **(*R,R*)-2a** by the hanging-drop vapor-diffusion method at 7°C. The protein solution contained 12 mg/ml GluR2-S1S2J-N775S in 10 mM HEPES (pH 7.0), 20 mM NaCl, and 1 mM EDTA. To this solution, an equal amount of ligand suspension containing 4.5 mM (*S*)-Glu, 22.5 mM **(*R,R*)-2a**, 10 mM HEPES (pH 7.0), 20 mM NaCl, 1 mM EDTA, and 10% DMSO was added. The protein-ligand suspension was left at 4°C for 1 week and was periodically shaken prior to crystallization experiments. Crystals were obtained in drops consisting of 2 μl protein-ligand suspension and 2 μl reservoir solution of 0.3 M $(NH_4)_2SO_4$, 0.1 M CH_3CO_2Na buffer (pH 5.5), and 25% PEG 4000. The reservoir volume was 0.5 ml. The crystals grew within 1 week to a maximum dimension of 0.1 mm.

Crystals of GluR2-S1S2J-N775S in complex with (*S*)-Glu and **(*R,R*)-2a** were transferred through reservoir solution containing ~20% glycerol prior to flash cooling in liquid nitrogen. A complete synchrotron data set was collected at beamline I911-2 at MaxLab, Lund, Sweden. Diffraction data were processed with the CCP4 programs MOSFLM and SCALA [32]. For crystal data and data collection statistics, see the Supplemental Data.

Two molecules (A and B) are present in the asymmetric unit of the crystal. The major part (91%) of the amino acid residues of both molecules A and B were traced with ARP/wARP [33] and the structure of the nondesensitizing GluR2 ligand-binding core mutant (S1S2J-L504Y) in complex with (*S*)-AMPA (PDB code: 1LB8; molecules A and B) for phasing the data. The remaining residues were built manually by using COOT [34], except for cloning remnant residues Gly-Ala and the C-terminal residues 790–792 and 795–796 of molecule A. Gln735 of molecule A and Met729 of molecule B were located in alternative conformations. Two (*S*)-Glu molecules, 1 **(*R,R*)-2a** molecule, 5 sulfate ions, 1 chloride ion, 2 glycerol molecules, and 523 water molecules were fitted into the electron density. The structure was refined by using program PHENIX [35]. Between each refinement step, the structure was inspected and corrected with COOT. The structure was refined to an R value of 16.8% and an R_{free} value of 23.2%. A summary of structure refinements is presented in Table S1.

The DynDom program [36] was employed for analysis of (*S*)-Glu-induced domain closure. The dimer interface was analyzed by using the Protein-Protein Interaction Server [37]. Figures were prepared with PyMOL [38].

Supplemental Data

Supplemental Data include descriptions of HPLC methods and apparatus and X-ray crystallography and are available at http://www.chembiol.com/cgi/content/full/14/11/1294/DC1/.

ACKNOWLEDGMENTS

H. Hald is gratefully acknowledged for providing protein for crystallization experiments, and P. Naur is acknowledged for help with cryomounting of the crystals and MaxLab during data collection. The work was supported by grants from The Dansync Center for Synchrotron Radiation and The Danish Medical Research Council.

Received: July 26, 2007
Revised: October 4, 2007
Accepted: October 5, 2007
Published: November 26, 2007

REFERENCES

1. Page, M.I., and Jencks, W.P. (1971). Entropic contributions to rate accelerations in enzymic and intramolecular reactions and the chelate effect. Proc. Natl. Acad. Sci. USA *68*, 1678–1683.
2. Jencks, W.P. (1981). On the attribution and additivity of binding energies. Proc. Natl. Acad. Sci. USA *78*, 4046–4050.
3. Murray, C.W., and Verdonk, M.L. (2002). The consequences of translational and rotational entropy lost by small molecules on binding to proteins. J. Comput. Aided Mol. Design *16*, 741–753.
4. Christopoulos, A., Grant, M.K.O., Ayoubzadeh, N., Kim, O.N., Sauerberg, P., and Jeppesen, L. (2001). Synthesis and pharmacological evaluation of dimeric muscarinic acetylcholine receptor agonists. Pharmacol. Exp. Ther. *298*, 1260–1268.
5. Soulier, J.-L., Russo, O., Giner, M., Rivail, L., Berthouze, M., Ongeri, S., Maigret, B., Fishmeister, R., Lezoualc'h, F., Sicsic, S., and Berque-Bestel, I. (2005). Design and synthesis of specific probes for human 5-TH_4 receptor dimerization studies. J. Med. Chem. *48*, 6220–6228.
6. Erez, M., Takemori, A.E., and Portoghese, P.S. (1982). Narcotic antagonistic potency of bivalent ligands which contain β-naltrexamine evidence for bridging between proximal recognition sites. J. Med. Chem. *25*, 847–849.
7. Portoghese, P.S. (1989). Bivalent ligands and the message — address concept in the design of selective opioid receptor antagonists. Trends Pharmacol. Sci. *10*, 230–235.
8. Halazy, S. (1999). G-protein coupled receptors bivalent ligands and drug design. Exp. Opin. Ther. Patents *9*, 431–446.
9. Armstrong, N., and Gouaux, E. (2000). Mechanism for activation and antagonism of an AMPA-sensitive glutamate receptor: crystal structures of the GluR2 ligand binding core. Neuron *28*, 165–181.
10. Hogner, A., Kastrup, J.S., Jin, R., Liljefors, T., Mayer, M.L., Egebjerg, J., Larsen, I.K., and Gouaux, E. (2002). Structural basis for AMPA receptor activation and ligand selectivity: crystal structures of five agonist complexes with the GluR2 ligand-binding core. J. Mol. Biol. *322*, 93–109.
11. Frandsen, A., Pickering, D.S., Vestergaard, B., Kasper, C., Nielsen, B.B., Greenwood, J.R., Campiani, G., Fattorusso, C., Gajhede, M., Schousboe, A., and Kastrup, J.S. (2005). Tyr702 is an important determinant of agonist binding and domain closure of the ligand-binding core of GluR2. Mol. Pharmacol. *67*, 703–713.
12. Hogner, A., Greenwood, J.R., Liljefors, T., Lunn, M.L., Egebjerg, J., Larsen, I.K., Gouaux, E., and Kastrup, J.S. (2003). Competitive antagonism of AMPA receptors by ligands of different classes: crystal structure of ATPO bound to the GluR2 ligand-binding core, in comparison with DNQX. J. Med. Chem. *46*, 214–221.
13. Kasper, C., Pickering, D.S., Mirza, O., Olsen, L., Kristensen, A.S., Greenwood, J.R., Liljefors, T., Schousboe, A., Watjen, F., Gajhede, M., et al. (2006). The structure of a mixed GluR2 ligand-binding core dimer in complex with (*S*)-glutamate and the antagonist (*S*)-NS1209. J. Mol. Biol. *357*, 1184–1201.
14. Sun, Y., Olson, R., Horning, M., Armstrong, N., Mayer, M., and Gouaux, E. (2002). Mechanism of glutamate receptor desensitization. Nature *417*, 245–253.
15. Jin, R., Clark, S., Weeks, A.M., Dudman, J.T., Gouaux, E., and Partin, K.M. (2005). Mechanism of positive allosteric modulators acting on AMPA receptors. J. Neurosci. *25*, 9027–9036.
16. Harpsøe, K., Liljefors, T., and Balle, T. (2007). Prediction of the binding mode of biarylpropylsulfonamide allosteric AMPA receptor modulators based on docking, GRID molecular interaction fields and 3D-QSAR analysis. J. Mol. Graph. Model.. Published online June 14, 2007. 10.1016/jmgm.2007.06.002.
17. Ornstein, P.L., Zimmerman, D.M., Arnold, M.B., Bleisch, T.J., Cantrell, B., Simon, R., Zarrinmayeh, H., Baker, S.R., Gates, M., Tizzano, J.P., et al. (2000). Biarylpropylsulfonamides as novel, potent potentiators of 2-amino-3-(5-methyl-3-hydroxyisoxazol-4-yl)-propionic acid (AMPA) receptors. J. Med. Chem. *43*, 4354–4358.
18. Quirk, J.C., and Nisenbaum, E.S. (2003). Multiple molecular determinants for allosteric modulation of alternatively spliced AMPA receptors. J. Neurosci. *23*, 10953–10962.

19. Jhee, S.S., Chappell, A.S., Zarotsky, V., Moran, S.V., Rosenthal, M., Kim, E., Chalon, S., Toublanc, N., Brandt, J., Coutant, D.E., and Ereshefsky, L. (2006). Multiple-dose plasma pharmacokinetic and safety study of LY450108 and LY451395 (AMPA receptor potentiators) and their concentration in cerebrospinal fluid in healthy human subjects. J. Clin. Pharmacol. *46*, 424–432.
20. Miller, W.D., Fray, A.H., Quatroche, J.T., and Sturgill, C.D. (2007). Suppression of a palladium-mediated homocoupling in a Suzuki cross-coupling reaction. Development of an impurity control strategy supporting synthesis of LY451395. Org. Process Res. Dev. *11*, 359–364.
21. Zarrinmayeh, H., Bleakman, D., Gates, M.R., Yu, H., Zimmerman, D.M., Ornstein, P.L., McKennon, T., Arnold, M.B., Wheeler, W.J., and Skolnick, P. (2001). [3H]N-2-(4-(N-Benzamido)phenyl)propyl-2-propanesulfonamide: a novel AMPA receptor potentiator and radioligand. J. Med. Chem. *44*, 302–304.
22. Shepherd, T.A., Aikins, J.A., Bleakman, D., Cantrell, B.E., Rearick, J.P., Simon, R.L., Smith, E.C.R., Stephenson, G.A., and Zimmerman, D.M. (2002). Design and synthesis of a novel series of 1,2-disubstituted cyclopentanes as small potent potentiators of 2-amino-3-(3-hydroxy-5-methyl-isoxazol-4-yl)propionic acid (AMPA) receptors. J. Med. Chem. *45*, 2101–2111.
23. Lee, P.H., Seomoon, D., and Lee, K. (2005). Palladium-catalyzed inter- and intramolecular coupling reactions of aryl and vinyl halides mediated by indium. Org. Lett. *7*, 343–345.
24. Morrow, J.A., Maclean, J.K.F., and Jamieson, C. (2006). Recent advances in positive allosteric modulators of the AMPA receptor. Curr. Opin. Drug Discov. Devel. *9*, 571–579.
25. Schrödinger, Inc. (2007). Maestro, Version 7.5.116 (http://www.shrodinger.com).
26. Schrödinger, Inc. (2007). Glide, Version 4.0.217 (http://www.shrodinger.com).
27. Schrödinger, Inc. (2007). MacroModel, Version 9.1.113 (http://www.shrodinger.com).
28. Liman, E.R., Tytgat, J., and Hess, P. (1992). Subunit stoichiometry of a mammalian K^+ channel determined by construction of multimeric cDNAs. Neuron *9*, 861–871.
29. Greenwood, J.R., Mewett, K.N., Allan, R.D., Martín, B.O., and Pickering, D.S. (2006). 3-Hydroxypyridazine 1-oxides as carboxylate bioisosteres: a new series of subtype-selective AMPA receptor agonists. Neuropharmacology *51*, 52–59.
30. Chen, G.Q., and Gouaux, E. (1997). Overexpression of a glutamate receptor (GluR2) ligand binding domain in Escherichia coli: application of a novel protein folding screen. Proc. Natl. Acad. Sci. USA *94*, 13431–13436.
31. Chen, G.Q., Sun, Y., Jin, R.S., and Gouaux, E. (1998). Probing the ligand binding domain of the GluR2 receptor by proteolysis and deletion mutagenesis defines domain boundaries and yields a crystallizable construct. Protein Sci. *7*, 2623–2630.
32. CCP4 (Collaborative Computational Project, Number 4) (1994). The CCP4 suite: programs for protein crystallography. Acta Crystallogr. D Biol. Crystallogr. *50*, 760–763.
33. Perrakis, A., Morris, R.M., and Lamzin, V.S. (1999). Automated protein model building combined with iterative structure refinement. Nat. Struct. Biol. *6*, 458–463.
34. Emsley, P., and Cowtan, K. (2004). Coot: model-building tools for molecular graphics. Acta Crystallogr. D Biol. Crystallogr. *60*, 2126–2132.
35. Adams, P.D., Grosse-Kunstleve, R.W., Hung, L.-W., Ioerger, T.R., McCoy, A.J., Moriarty, N.W., Read, R.J., Sacchettini, J.C., Sauter, N.K., and Terwilliger, T.C. (2002). PHENIX: building new software for automated crystallographic structure determination. Acta Crystallogr. D Biol. Crystallogr. *58*, 1948–1954.
36. Hayward, S., and Berendsen, H.J.C. (1998). Systematic analysis of domain motions in proteins from conformational change; new results on citrate synthase and T4 lysozyme. Proteins Struct. Funct. Genet. *30*, 144–154.
37. Jones, S., and Thornton, J.M. (1996). Principles of protein-protein interactions derived from structural studies. Proc. Natl. Acad. Sci. USA *93*, 13–20.
38. Delano, W.L. (2002). The PyMOL Molecular Graphics System (San Carlos, CA: Delano Scientific).

Accession Numbers

Coordinates have been deposited in the RCSB Protein Data Bank under accession code 3BBR.